Journal of Materials Chemistry A

Accepted Manuscript

ROYAL SOCIETY OF CHEMISTRY

www.rsc.org/materialsA

Journal Name

ARTICLE

Frequency-regulated Pulsed Electrodeposition of $CuInS_2$ on ZnO Nanorod Arrays as Visible Light Photoanodes

Received 00th January 20xx,
Accepted 00th January 20xx

DOI: 10.1039/x0xx00000x

www.rsc.org/

Yiming Tang, Peng Wang, Jung-Ho Yun, Rose Amal*, and Yun Hau Ng*

Vertically aligned ZnO nanorod arrays on fluorine doped tin oxide (FTO) substrate were uniformly-coated with visible light active $CuInS_2$ nanoparticles using electrodeposition regulated by an optimized frequency. As the diffusion of fresh metallic precursor to the bottom of the one-dimensional nanostructure is the major challenge during electroposition, frequency tuning has demonstrated its effectiveness in balancing the diffusion and deposition of the secondary component ($CuInS_2$) on the one-dimensional substrate (ZnO). The high quality of heterojunction between $CuInS_2$ and ZnO together with its intimate interaction facilitated efficient charge shuttling from $CuInS_2$ to ZnO to yield four-fold visible light response compared with the traditionally-made $CuInS_2$-ZnO nanostructures.

Introduction

Photosensitisation of nanocrystalline wide band gap oxide semiconductors is a well-established strategy that facilitates charge injection from a sensitizer to the wide band gap semiconductors to allow photoelectrochemical and photocatalytic reactions upon visible light illumination.[1] The sensitizers are typically refers to those optically excited components such as organic dye molecules, plasmonic metal and inorganic narrow band gap semiconductors (< 2.9 eV).[2-4] Partly because of the highly energetic valence and conduction bands, the most redox-active semiconductors reported to date have been mainly UV-triggered metal oxides, such as TiO_2, ZnO, $SrTiO_3$ and Ta_2O_5.[5-7] Limited by their intrinsic wide optical band gap that typically requires high energy photon to activate, photosensitization appears to be the most effect way to extend the photoactivity of a wide band gap oxide into visible light region without engineering its energetic band energy that might affect the redox capability. Functionalization of wide band gap oxides with narrow band gap semiconductor is commonly seen in today's development of photoactive composite materials.[8, 9] Methodologies employed are depending on the physical status of the wide band gap oxides: powder (i.e. colloidal suspension) or thin film. Effective ways in attaching, decorating, or coating powdered wide band gap oxides (e.g. TiO_2 and ZnO) with the inorganic sensitizers include hydrothermal treatment, ion-exchange, photoreduction and etc.[10-13] On the other hand, for wide band gap materials in the form of flat thin film, the sensitizers are usually introduced using thermal evaporation,[14] spin-coating,[15] chemical bath growth,[16] successive ionic layer adsorption and reaction (SILAR),[17] and electrodeposition.[18] In the case of conventional thin film in which smooth and flat surface is the typical morphology, all the above mentioned methods are useful and some of them are also cost-effective (e.g. electrodeposition). Because of its low cost and simplicity, electrodeposition of secondary semiconductor on TiO_2 and ZnO films has been extensively reported.[19-21] The latest development of photoactive thin film, however, often inclines to the anisotropic formation of wide band gap oxide nanostructures (e.g. vertically aligned nanotubes, nanorods and nano-needle) on the flat substrate. It is generally accepted that the anisotropic growth of oxide can reduce the light-loss through surface reflection as well as to increase the contact area with reactants in the solution or electrolyte. Although advantages are obvious, the non-even surface of the wide band gap oxide thin film imposes great challenge to introduce the inorganic sensitizer as the secondary component of the thin film using conventional electrodeposition. It is even more challenging when the secondary inorganic sensitizer is not a binary but ternary semiconductor.

In the film configuration of nanorods and nanotubes, it is difficult to achieve homogeneous coating from the tip to the bottom of the one-dimensional nanostructures. The presence of concentration gradient of the precursor throughout the film promotes the accumulation of the secondary semiconductor on the top region (or entrance) of the nanorods/nanotubes. A compact layer of secondary semiconductor completely covering the upper sections of the nanostructures, as a result, diminishes the advantages of being one-dimensional. We have recently developed a unique electrodeposition method by introducing a square-wave pulsing condition during the

Particles and Catalysis Research Group, School of Chemical Engineering, The University of New South Wales, Sydney NSW 2052, Australia.
**Corresponding authors: r.amal@unsw.edu.au; yh.ng@unsw.edu.au*
† Footnotes relating to the title and/or authors should appear here.
Electronic Supplementary Information (ESI) available: [details of any supplementary information available should be included here]. See DOI: 10.1039/x0xx00000x

electroplating of secondary semiconductor on TiO_2 nanotube and ZnO nanorod arrays.[22, 23] The pulse-electrodeposition consists of two main components: (1) relaxation voltage (0 V) and (2) depositing voltage (cathodic range, i.e. negative V). While depositing voltage induces nucleation and deposition of the secondary component, the relaxation voltage allows fresh precursor to diffuse through the bottom of the nanorods/nanotubes and nucleated upon the subsequent depositing voltage. These repeated cycles of relaxation-deposition voltages eventually enable the quality coating of the nanorods/nanotubes. However, there is no universal pulsing condition for all one-dimensional nanostructures. This is because the relaxation setup for the diffusion of precursor is depending on the geometry of the nanostructures (i.e. tubes/rods, void diameter and oxide thickness). The viscosity of electrolyte and the concentration of the precursors can be the two parameters to achieve a balance diffusion-deposition relationship.[24, 25] In this work, we demonstrate the pulsing frequency as an effective tool to regulate the uniform coating of ZnO nanorod arrays with $CuInS_2$ nanoparticles. Frequencies at both extreme high and low ends (1 MHz and 1 Hz respectively) are detrimental to the electrodeposition as the nucleation and deposition are either too fast or lengthy. An appropriate pulsing frequency is crucial in ensuring a balanced equilibrium between diffusion and cathodic deposition of the $CuInS_2$ precursors. The sufficient access to the fresh $CuInS_2$ precursors at the bottom of the ZnO nanorod arrays result in the well-coated $CuInS_2$-ZnO nanocomposite film. This complete coatings as well as the intimate interaction between ZnO nanorods and $CuInS_2$ facilitate efficient electron injection from $CuInS_2$ to ZnO for four-fold photoelectrochemical activity than the conventional $CuInS_2$-ZnO thin film.

Experimental

Preparation of a ZnO nanorod film on a FTO substrate

A ZnO nanorod film was prepared by a chemical bath deposition (CBD) method on a FTO substrate. The FTO substrates were pre-cleaned with Milli-Q water, ethanol (99.5%, Sigma-Aldrich) and acetone (99.8%, Chem-Supply) under mild sonication followed by drying in vacuum before use. Several drops of a solution containing 0.005 M of zinc acetate (Ajax Finechem) dissolved in ethanol were applied on the transparent FTO substrates. After 10 seconds, the substrate was rinsed with ethanol and dried with nitrogen gas. The dropwise process with zinc acetate was repeated for five times before calcined for 20 min at 350 °C to form ZnO seeds from thermal decomposition of zinc acetate. The whole seeding procedure was repeated for two times to obtain an evenly distributed ZnO seed layer on the FTO substrate.

The seeded substrate was sealed in a scotch bottle with 100 mL aqueous solution consisted of half 0.05 M of zinc nitrate (98%, Sigma-Aldrich) and half 0.05 M of hexamethylenetetramine (99%, Sigma-Aldrich) used as a structure-directing agent.[26] Each solution was preheated to 90°C for 5 min before mixing together to speed up the reaction in the CBD process. The bottle was then kept in the oven at 90°C for 3 h for one growth cycle and repeated for two times with fresh solutions. The obtained ZnO nanorod thin films were rinsed thoroughly in Milli-Q water and dried in air. At last, the transparent ZnO nanorod film was calcined for 30 min at 450 °C to completely remove the remaining organic components.

Preparation of $CuInS_2$ nanoparticles on the ZnO nanorod film

$CuInS_2$ nanoparticles on the ZnO nanorod film were deposited by a sequential pulsed-electrodeposition method developed in our previous work.[22] We chose a two-electrode system for electrodeposition consisted of the resultant ZnO/FTO film from CBD as the working electrode and a Pt foil as the counter electrode. A mixture of 10 mM $CuCl_2$ and 100 mM $Na_2S_2O_3$ was chosen for the electrolyte in the first step and 10 mM $InCl_3$ in the second step. The duration of each step was 10 min. The $CuInS_2$ nanoparticles was deposited electrochemically by applying a repetitive on-off time square pulse generated by a functional generator (TG4001, Thurlby Thandar Instruments), applying a cathodic pulse (-1.25 V, 100 ms) and short-circuit pulse (0 V, 100 ms) alternatively. Three different frequencies, 1 Hz, 1 kHz and 1 MHz, were adapted for comparison. The-obtained $CuInS_2$-ZnO film was dried and annealed at 500 °C for 1 h in a gas mixture of 92% N_2 and 8% H_2 to facilitate crystallization. Before the heating, N_2 was purged through the tube furnace for 2 h to completely remove the air. Subsequently, the heating was performed with the ramping rate of 5 °C/min from room temperature to 500°C. The gas flow rate was maintained at 50 mL/min throughout the process.

Characterization of the obtained $CuInS_2$-ZnO films

The crystallographic phase structures of the deposited films were characterized using an X-ray diffractometer (X'pert Pro MRD, Philips) with Cu K_α radiation at 45 kV and 40 mA, a step size of 0.013° and a scan step time at 97.92 s in the 2θ range of 25° to 60°. The morphological features and the film thickness were determined using a scanning electron microscope (SEM, S900 Hitachi). The UV-Vis diffuse reflectance spectra were obtained using a UV/Vis/NIR spectrophotometer (Perkin Elmer LAMBDA 1050) with GaP (1200-900nm) and Si (900-250nm) detectors. A high-resolution transmission electron microscopy (HRTEM, CM 200 Philips) was employed to examine the lattice fringes of electrodeposited $CuInS_2$ and ZnO crystals, as well as the interface between the $CuInS_2$ nanoparticles and the ZnO nanorod film. The photoluminescence emission spectra were obtained using a spectrometer (FluoroMax-4, Horiba) to study the electron-hole recombination rate in the film.

Photoelectrochemical (PEC) characterization

The photoelectrochemical properties of the $CuInS_2$-ZnO films were examined under potentiostatic conditions in a three-electrode system using $CuInS_2$-ZnO films as the working electrode, Ag/AgCl as the reference electrode and a platinum

wire as the counter electrode in an aqueous solution containing 0.25 M of Na_2S and 0.35 M of Na_2SO_3 at pH 12. An electrolytic cell made out of Teflon with a flat quartz window was used. The photocurrent responses were measured under visible light illumination using a 300 W Xenon lamp with a cut off filter (λ ≥ 435 nm). The illuminated area of the working electrode was fixed at 0.196 cm^2.

Results and Discussion

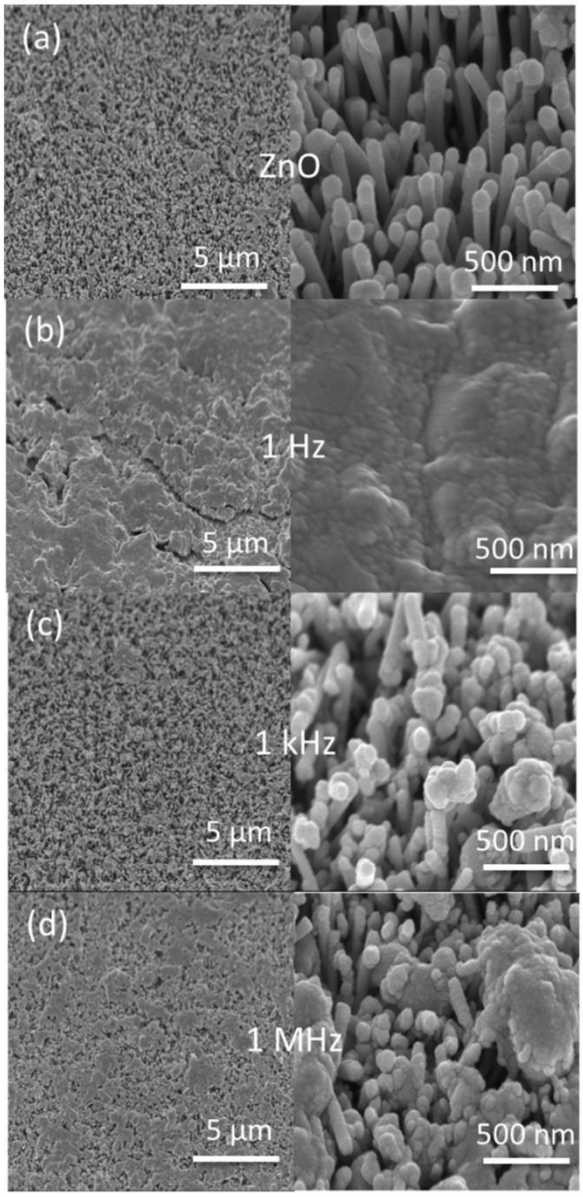

Figure 1 SEM images of (a) bare ZnO nanorods and $CuInS_2$-ZnO composites prepared using (b) 1 Hz, (c) 1 kHz and (d) 1 MHz in the pulsed electrodeposition (cathodic voltage: -1.25 V; relaxation voltage: 0 V) (+30° tilted view).

Morphological features of bare ZnO nanorods and $CuInS_2$-ZnO nanocomposites prepared using low, medium and high frequencies were examined by SEM (Figure 1). Upon chemical bath synthesis with calcination treatment, a dense, clean and smooth nanorods array is seen on the FTO substrate as shown in Figure 1a. XRD (Figure S1 in the supplementary Information) verifies these nanorods as crystalline ZnO. The subsequent pulsed-electrodeposition step introduced the $CuInS_2$ nanoparticles onto the ZnO nanorods with the aim of uniformly wrapping the whole surface of ZnO nanorods. The principle pulsed-electrodeposition condition had been carefully developed to minimise the chemical dissolution of ZnO nanorods in the slightly acidic electrolyte.[22] All Figures 1(b-d) indicate the presence of deposit on ZnO with varied coating quality in which these deposits are later confirmed as $CuInS_2$ using HRTEM and UV-Vis absorption spectroscopy. Note that although the crystalline $CuInS_2$ can also be detected by XRD (Figure S1), the overall peak intensity is too low as ZnO is the dominant phase in the composite. At low frequency (1 Hz), the typical morphological feature of ZnO nanorods is replaced by the nearly-compact layer of $CuInS_2$ located on top of the nanoarrays. While the junction of $CuInS_2$ top-layer and the ZnO nanorods under-layer is still formed at the interface and can facilitate charge transfer upon photoexcitation, the heterojunction is poor where most of the underneath ZnO nanorods are undecorated and the photogenerated electrons in the thick $CuInS_2$ layer will encounter limitless grain boundaries. At high frequency (1 MHz), nanoparticles of $CuInS_2$ are coated on ZnO nanorods with certain extent of $CuInS_2$ aggregation on the top region of ZnO nanorods. This aggregation of $CuInS_2$ is more apparent under the lower magnification examination. Nearly half of the examined area demonstrates the closure of entrance into deeper region of the nanorods. In contrast, at moderate frequency of 1 kHz, typical ZnO nanorods morphology is retained with clear roughness observed on the surface of ZnO. The rough surface indicates the deposition of $CuInS_2$ nanoparticles. The mechanisms contribute to the variation of coating, obviously, lie on the pulsing condition.

Figure 2 depicts the TEM and HRTEM images of bare ZnO nanorods and $CuInS_2$-ZnO nanocomposites derived from different frequencies. Bare ZnO powder scratched off from the FTO substrate presents rod-like structures with diameter of ca. 45-50 nm which matches well with the SEM observation. The nanorods have well-defined surface and edges. Lattice fringe of 0.26 nm measured under HRTEM analysis confirms it is the (001) facet of ZnO. Upon pulsed-electrodeposition at 1 KHz, the overall nanorods surface turned coarse and uneven with slightly enlarged nanorod diameter of ca. 50-55 nm, suggesting the deposition of secondary component. A careful scrutiny on the surface revealed that irregularly-shaped $CuInS_2$ nanoparticles, with lattice fringe of 0.32 nm corresponding to (112) facet, were homogeneously present at the interface of (001) ZnO. In other words the ZnO nanorods were uniformly "wrapped" by the electrodeposited $CuInS_2$. In comparison, when $CuInS_2$-ZnO derived from 1 Hz was examined, large clusters of $CuInS_2$ nanoparticles were found individually separated from the ZnO nanorod. The surface of this 1 kHz-made $CuInS_2$-ZnO nanorods were largely clean and smooth as the bare ZnO. Interface of ZnO and $CuInS_2$ was mainly found on the tip of nanorods as shown in Figure 2f. Comparable interface quality was observed in the $CuInS_2$-ZnO nanocomposites prepared at 1 MHz pulsing condition.

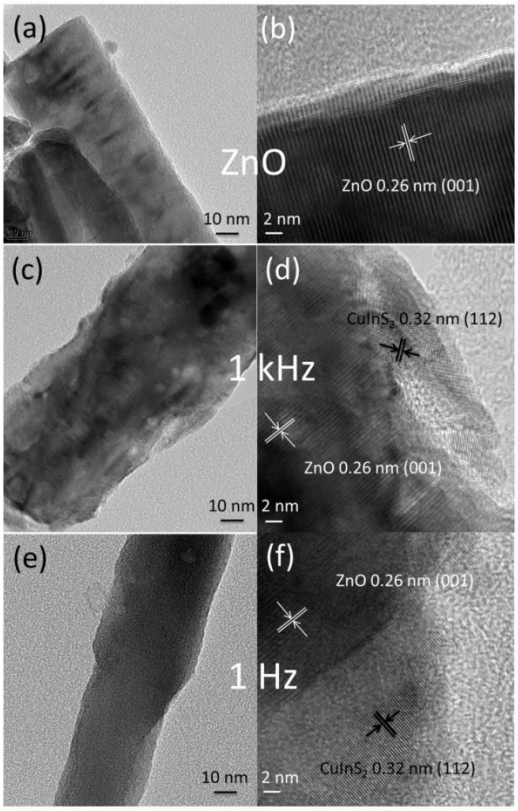

Figure 2. TEM and HRTEM images of (a-b) ZnO and $CuInS_2$-ZnO composites using (c-d)) 1 kHz and (e-f) 1Hz of frequencies in the pulsed-electrodeposition (cathodic voltage: -1.25 V; relaxation voltage: 0 V).

During pulsed-electrodeposition, two distinct layers are formed near the surface of electrodes, namely pulsating diffusion layer and stationary diffusion layer (Figure 3).[27, 28] The cationic precursors from the electrolyte are driven to the electrode by cathodic voltage and subsequently reduced to compose a thin deposit layer on the film. The concentration of precursors closer to the substrate is therefore depleting accordingly. This depletion zone is replenished by fresh metallic precursors from the bulk solution (far from the substrate) and equilibrium is achieved to allow the continuing deposition of the precursors. This mechanism applies to both traditional and pulsed-electrodeposition. In the case of one-dimensional nanorods substrate, however, the mass transport of the precursor to the bottom of nanostructure is challenged by its length and the capillary resistance. By introducing a pulse in electrodeposition, the diffusion of precursors to the bottom of the nanorod arrays is controlled to allow deposition throughout the length of the nanorods. An equilibration of precursor diffusion and deposition has to be achieved for the uniform coating of ZnO nanorods. At low frequency (1 Hz) pulsed-electrodeposition in which the duration of cathodic voltage was sufficiently long, the nucleation and growth of the $CuInS_2$ occurred faster on the tip of ZnO nanorods because the precursors at the bottom region were consumed but not replenished effectively. This eventually blocked the entrance of the nanorod arrays. The bottom layer of the nanorods had no or limited access to the fresh precursors from the bulk electrolyte. As a result, the subsequent deposition of $CuInS_2$ was built up on the $CuInS_2$ and this yielded a distinct compact layer of $CuInS_2$ on top of most nanorod arrays (as shown in Figure 1b). A low frequency pulsed-electrodeposition is therefore analogous to the non-pulsed system where the cathodic voltage is supplied continuingly. Under suitable frequency (1 kHz), the brief cathodic voltage (-0.1 V) induced the nucleation and deposition of $CuInS_2$ on ZnO nanorod. The following relaxation voltage (0 V) allowed time for the diffusion of fresh precursors from the pulsating diffusion layer to the interstices of the nanorods. The decreased concentration of precursor in the pulsating layer was then equilibrated by the static diffusion layer. The repeating cycles of deposition and diffusion process finally resulted in the uniform coating of the ZnO nanorods. In comparison, at high frequency (1 MHz), though the short cathodic voltage duration did not induce significant closure of the nanorods entrance, its brief relaxation time (1 μs) did not facilitate sufficient diffusion throughout the nanorods and therefore decoration of top region of ZnO was observed (Figure 1d). Note that the suitable frequency found in this work is subject to the geometry of the nanoarrays and therefore pulse-condition for each nanostructure (e.g. nanotubes with different density or pore size) should be optimised.

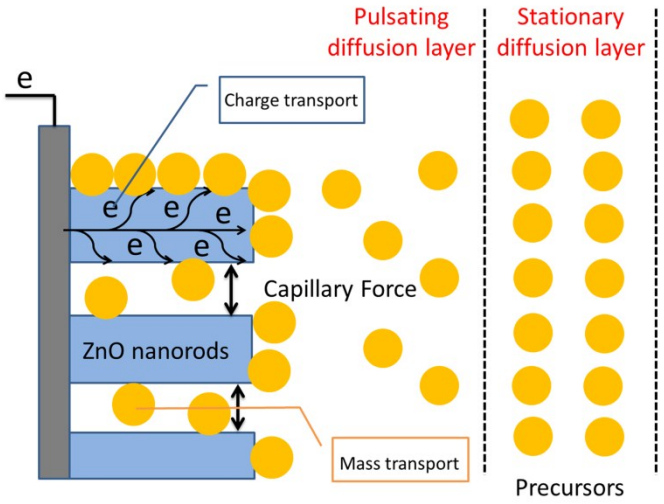

Figure 3. Schematic illustration of the mass transport and charge transport during the pulsed-electrodeposition of $CuInS_2$ on ZnO nanorods.

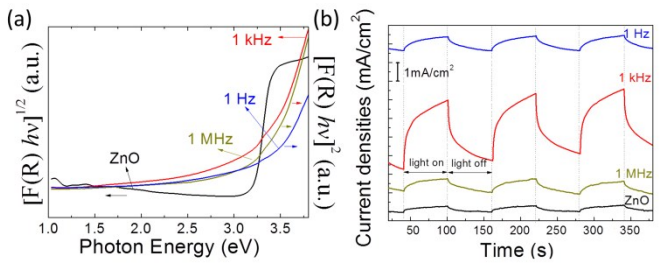

Figure 4 (a) Tauc plots of ZnO and $CuInS_2$-ZnO composites at different frequencies in the pulsed electrodeposition; and (b) visible light response of $CuInS_2$-ZnO composites at 0.5 V vs Ag/AgCl in an electrolyte containing 0.25 M Na_2S and 0.35 M Na_2SO_3 (pH = 12) under repeated on-off illumination cycles (λ ≥ 435 nm).

The Tauc plots of ZnO nanorods and $CuInS_2$-ZnO nanocomposites are displayed in Figure 4a. The ZnO nanorod, which is an UV-active material, shows negligible absorption in the visible-light range. The absorption edge is around 380 nm, corresponding to the band gap energy value of ZnO (3.25 eV). Upon coating with $CuInS_2$ nanoparticles from pulsed electrodeposition regardless the frequencies applied, the absorption edges of $CuInS_2$-ZnO composites extended to a longer wavelength up to 820 nm (1.51 eV), demonstrating the formation of visible light active $CuInS_2$. $CuInS_2$-ZnO nanocomposites using different frequencies of 1 Hz, 1 kHz and 1 MHz show similar absorption profiles. Figure 4b illustrates the amperometric photocurrent generation of the ZnO and $CuInS_2$-ZnO films upon visible light irradiation. Bare ZnO nanorod arrays exhibit negligible visible light response. All $CuInS_2$-ZnO samples presented anodic photocurrent, indicating the n-type conductivities of all thin films.[29] Although the photoresponses were reproducible during the illumination cycles, the relatively slow photoresponses compared to common oxide-based photoactive materials such as ZnO and TiO_2 are associated with the intrinsic photocorrosion of sulphide materials. Previous studies on $CuInS_2$ photoelectrode have shown that the application of polysulphide electrolyte supresses the photocorrision of $CuInS_2$ during measurement.[29] While all $CuInS_2$-ZnO nanocomposite films show visible light activities, the sample derived from 1 kHz demonstrates remarkably higher photocurrent (3.5 mA/cm^2) than that of the 1 Hz (~0.8 mA/cm^2) and 1 MHz (~0.8 mA/cm^2). As the deposited amount of $CuInS_2$ was comparable among all thin films, the differences in visible light responses were attributed to the quality of the interface between $CuInS_2$ and ZnO.

Coupling ZnO with narrow band gap $CuInS_2$ can extend the light response into visible region (as shown in Figure 4a). The extent of the visible light photocurrent, however, is determined by the population of charges being transferred from $CuInS_2$ to ZnO, in which the quantity of the charge transfer is greatly influenced by the quality of the $CuInS_2$-ZnO interface. Figure 5 (a) depicts the morphological feature of $CuInS_2$-ZnO nanocomposites obtained from the appropriate frequency and the uncontrolled experimental conditions, respectively. The effective contact area between $CuInS_2$ and ZnO is significantly varied among the samples. The well-coated 1 kHz film was beneficial from the intimate interaction where the photogenerated electrons in $CuInS_2$ were efficiently injected into the conduction band of ZnO.[30] Owing to the high electron mobility of ZnO (200-300 cm^{2}Vs^{-1}), these electrons were transported to the FTO and subsequently to the counter electrode to generate photocurrent. For the non-optimised frequencies as well as non-pulsing condition, the formation of compact $CuInS_2$ layer or severe accumulation of $CuInS_2$ particles at the entrance of the nanorod arrays (the tips) impaired the charge transfer. Although $CuInS_2$ was photoexcited, the electrons encountered limitless grain boundaries before reaching ZnO. The charges experienced recombination before being extracted to the photoelectrochemical circuit.

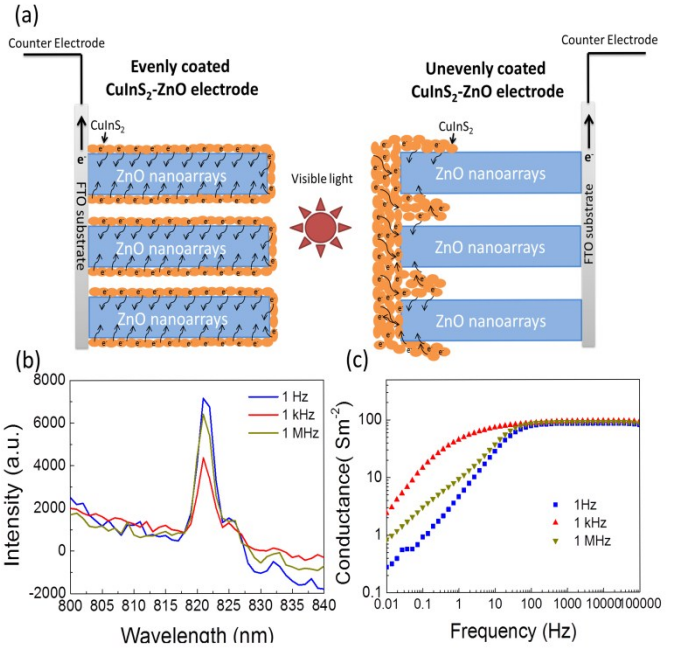

Figure 5 (a) Schematic illustration of the photocharge transportation of $CuInS_2$-ZnO nanocomposites; (b) photoluminescence (PL) emission spectra of $CuInS_2$-ZnO nanocomposites with excitation wavelength of 775 nm light; (c) Conductance plots of $CuInS_2$-ZnO nanocomposites obtained under visible light illumination (λ ≥ 435 nm) at 0.1 V vs Ag/AgCl from 10 mHz to 100 kHz.

The higher charge recombination rates in $CuInS_2$-ZnO nanocomposites obtained at 1 Hz and 1 MHz are reflected in their photoluminescence spectra (PL) (Figure 5b). When the excited electrons in $CuInS_2$ returned to their ground states (recombination), the energy emitted from this relaxation can be observed in the form of luminescence. Therefore, in most cases, the intensity of the PL peak is proportional to the degree of charge recombination. The well-coated $CuInS_2$-ZnO derived from 1 kHz clearly demonstrates its lowest PL emission peak intensity. The efficient electron transfer to ZnO rendered fewer electrons for recombination. Note that the emission peak at 821 nm is also equivalent to the 1.5 eV band gap of $CuInS_2$ and therefore there was no PL peak observed in the bare ZnO at this wavelength. In addition to the charge recombination insight, conductance of the $CuInS_2$-ZnO films provides useful information on the overall electrons transport

throughout the nanostructures. Figure 5c shows the conductance plots of the $CuInS_2$-ZnO thin films measured under visible light illumination. Conductance measured at higher frequency (>100 Hz) is attributed to the electrolyte and therefore the value was identical for all thin films. The conductance of the nanocomposites was indicated in the frequency ranged from 0.1 to 100 Hz while at the extreme low frequency at 0.1 Hz the conductance of the ZnO-FTO interface was evaluated. Under visible illumination, the highest conductance was observed on the $CuInS_2$-ZnO obtained at 1 kHz. In general, all illuminated $CuInS_2$-ZnO films have greater values of conductance than bare ZnO (data not shown). The quantity of electrons transferred from $CuInS_2$ to ZnO under visible light illumination appears to contribute to the overall conductance enhancement of ZnO.

Conclusions

Uniform coating of vertically-aligned ZnO nanorods by ternary semiconductor of $CuInS_2$ were achieved using a frequency-regulated pulsed-electrodeposition. The applied frequency during the electrodeposition was a key factor in controlling the two crucial coating mechanisms over one-dimensional nanostructures: diffusion of precursors and cathodic reduction of the metallic precursors. The absence of sufficient diffusion time in the traditional or non-optimised pulsed electrodeposition leads to the ineffective coating of ZnO. The complete coatings as well as the close interaction between ZnO nanorods and $CuInS_2$ components are the two important aspects to facilitate efficient electron transfer for greater photoelectrochemical performances. The $CuInS_2$-ZnO film derived from the optimised frequency synthesis showed remarkably four times greater photoresponse. The success of using frequency to regulate coating quality on anisotropic oxide demonstrates the versatility of electrodeposition technique to evenly coat other non-flat substrates.

Acknowledgements

This work has been supported by the Australian Research Council Discovery Project (DP110101638). Yiming Tang acknowledges the China Scholarship Council scholarship. Professor Gavin Conibeer from School of Photovoltaics and Renewable Energy Engineering is acknowledged for the support of the access to UV/Vis/NIR spectrophotometer. The authors acknowledge the UNSW Mark Wainwright Analytical Centre for the SEM and TEM equipment and technical support.

Notes and references

1. C. A. Bignozzi, R. Argazzi and C. J. Kleverlaan, *Chem. Soc. Rev.*, 2000, **29**, 87.
2. J- H. Yun, Y. H. Ng, C. Ye, A. J. Mozer, G. G. Wallace and R. Amal, *ACS Appl. Mater. Interfaces*, 2011, **3**, 1585.
3. K. Li, B. Chai, T. Peng, J. Mao and L. Zan, *ACS Catal.*, 2013, **3**, 170.
4. Y. Hou, F. Zuo, A. Dagg and P. Feng, *Nano Lett.*, 2012, **12**, 6464.
5. Y. H. Ng, S. Ikeda, M. Matsumura and R. Amal, *Energy Environ. Sci.*, 2012, **5**, 9307.
6. J. Zhang, J. H. Bang, C. Tang and P. V. Kamat, *ACS Nano*, 2010, **4**, 387.
7. A. Dabirian and R. van de Krol, *Chem. Mater.*, 2015, **27**, 708.
8. C. Ng, A. Iwase, Y. H. Ng and R. Amal, *J. Phys. Chem. Lett.*, 2012, **3**, 913.
9. H. Zhang, X. Quan, S. Chen, H. Yu and N. Ma, *Chem. Mater.*, 2009, **21**, 3090.
10. J. Yu, W. Wang, B. Cheng and B.-L. Su, *J. Phys. Chem. C*, 2009, **113**, 6743.
11. H. Tian, X. L. Zhang, J. Scott, C. Ng and R. Amal, *J. Mater. Chem. A*, 2014, **2**, 6432.
12. V. Puddu, R. Mokaya and G. Li Puma, *Chem. Commun.*, 2007, 4749.
13. F. M. Courtel, R. W. Paynter, B. Marsan and M. Morin, *Chem. Mater.*, 2009, **21**, 3752.
14. O. Bondarchuk, X. Huang, J. Kim, B. D. Kay, L.-S. Wang, J. M. White and Z. Dohnálek, *Angew. Chem. Int. Ed.*, 2006, **45**, 4786.
15. J. Jinmyoung, K. Darae, Y. Dong-Jin, J. Hwichan, R. Shi-Woo, L. Jae Sung, Y. Kijung, K. Sungjee and J. Sangmin, *Nanotechnology*, 2010, **21**, 325604.
16. W. Lee, S. K. Min, V. Dhas, S. B. Ogale and S.-H. Han, *Electrochem. Commun.*, 2009, **11**, 103.
17. Y. Tak, S. J. Hong, J. S. Lee and K. Yong, *J. Mater. Chem.*, 2009, **19**, 5945.
18. J. Miao, H. B. Yang, S. Y. Khoo and B. Liu, *Nanoscale*, 2013, **5**, 11118.
19. N. Detacconi, C. Chenthamarakshan, K. Rajeshwar, T. Pauporte and D. Lincot, *Electrochem. Commun.*, 2003, **5**, 220.
20. J. Katayama, K. Ito, M. Matsuoka and J. Tamaki, *J Appl. Electrochem.*, 2004, **34**, 687.
21. T. Yoshida, J. Zhang, D. Komatsu, S. Sawatani, H. Minoura, T. Pauporté, D. Lincot, T. Oekermann, D. Schlettwein, H. Tada, D. Wöhrle, K. Funabiki, M. Matsui, H. Miura and H. Yanagi, *Adv. Funct. Mater.*, 2009, **19**, 17.
22. Y. Tang, J. H. Yun, L. Wang, R. Amal and Y. H. Ng, *Dalton Trans.*, 2015, **44**, 7127.
23. J. H. Yun, Y. H. Ng, S. Huang, G. Conibeer and R. Amal, *Chem. Commun.*, 2011, **47**, 11288.
24. G. Gonzalez, G. Marshall, F. V. Molina, S. Dengra and M. Rosso, *J. Electrochem. Soc.*, 2001, **148**, C479.
25. J. F. K. Cooper, K. N. Vyas, J. J. Palfreyman and C. H. W. Barnes, *Electrochem. Commun.*, 2013, **27**, 96.
26. L. Vayssieres, K. Keis, S.-E. Lindquist and A. Hagfeldt, *J. Phys. Chem. B*, 2001, **105**, 3350.
27. N. Ibl, J. C. Puippe and H. Angerer, *Surf. Technol.*, 1978, **6**, 287.
28. J. C. Puippe and N. Ibl, *J Appl. Electrochem.*, 1980, **10**, 775.
29. Y. Tang, Y. H. Ng, J. H. Yun and R. Amal, *RSC Adv.*, 2014, **4**, 3278.
30. Y. Li, Z. Liu, Y. Wang, Z. Liu, J. Han and J. Ya, *Int. J. Hydrogen Energ.*, 2012, **37**, 15029.

Table of Contents

Frequency-regulated Pulsed Electrodeposition of $CuInS_2$ on ZnO Nanorod Arrays as Visible Light Photoanodes

Yiming Tang, Peng Wang, Jung-Ho Yun, Rose Amal* and Yun Hau Ng*

Particles and Catalysis Research Group, School of Chemical Engineering, The University of New South Wales, Sydney NSW 2052, Australia.
*Corresponding author: Email; r.amal@unsw.edu.au; yh.ng@unsw.edu.au

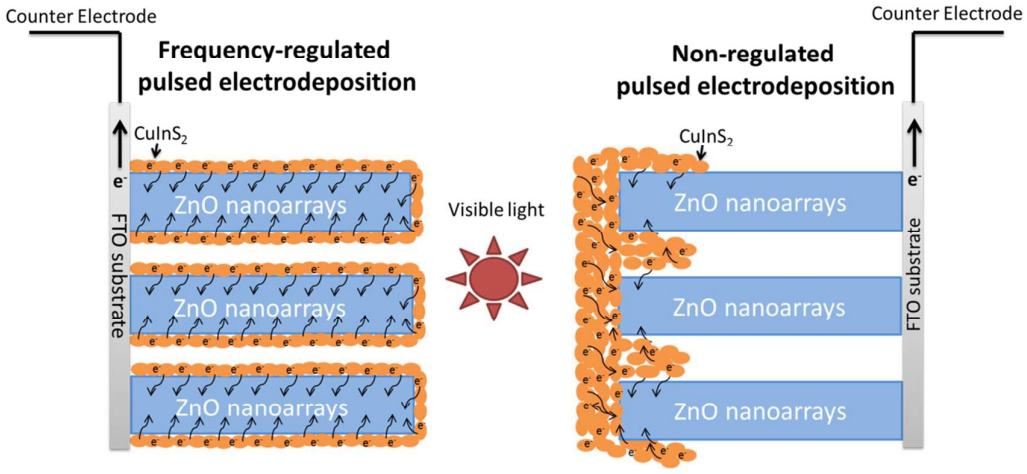

High quality coating of vertically aligned ZnO nanorods with $CuInS_2$ nanoparticles is achieved by a pulse-regulated electrodeposition method.